Mecánica Computacional Vol. XXI, pp. 586–604
S. R. Idelsohn, V. E. Sonzogni and A. Cardona (Eds.)
Santa Fe–Paraná, Argentina, October 2002

GENERIC PROPERTIES OF THE SOLUTIONS OF THE TWO-FLUID MODEL IN LAMINAR FULLY-DEVELOPED TWO-PHASE FLOW

Osvaldo E. Azpitarte and Gustavo C. Buscaglia

Centro Atómico Bariloche and Instituto Balseiro
8400 Bariloche, Argentina

Key Words: Two-phase flow, bubbly flows, two-fluid model

Abstract. *An analysis of the solutions of the two-fluid model for vertical fully-developed flow is conducted. The resulting equation system is reduced to a single ordinary differential equation (ODE). Introducing an intrinsic length scale L deduced form the system, which value is approximately that of the bubble radius, the ODE is rendered non-dimensional. With the aid of this equation, some generic properties of the solutions of the model for pipes with diameter greater than about 20 L (the usual case) are found. Firstly the central region of the pipe, where wall efects vanish, is considered. It is proved that an almost exact compensation of the applied pressure gradient with the hydrostatic force* $\rho_{eff}\,\mathbf{g}$ *occurs (with* ρ_{eff} *the effective density and* $\mathbf{g}$ *the gravity). This compensation implies that flat void fraction and velocity profiles are the only possible solutions in the central region, and that the void fraction at the center of the pipe only depends on the pressure gradient.*

Finally, the complete problem is considered with a numerical approach, with the effect of the wall dealt via wall forces. The previous mathematical results are confirmed and the near-wall phase distributions and velocity profiles are found. With the numerical code it is also possible to investigate the regime in which the pressure gradient is greater than the weight of the pure liquid, in which case a region of strictly zero void fraction develops, surrounding the axis of the pipe (in upward flow of bubbles), or at the wall of the pipe (in downward flow of bubbles).

1 INTRODUCTION

The two-fluid model (Ishii, 1975)[6] is, at present, widely used in the simulation of two-phase flows. It emerges from the exact conservation equations after ensemble averaging, introducing unknowns such as the phase fraction $\epsilon_k(\mathbf{x}, t)$, which is the probability of finding phase k at the position $\mathbf{x}$ at time t. The ensemble averaging process needs to be complemented with several closure relations which are far from established, either conceptually or quantitatively. For example, the lift term modeling transversal forces that act upon bubbles or particles in the presence of a velocity gradient, is not completely understood. The effective lift coefficient for bubbles that fits pipe-flow data ($C_L \simeq 0.05$; Lahey, 1990)[7] is much smaller than that deduced from potential flow calculations ($C_L = \frac{1}{2}$; Drew & Lahey, 1987)[4], while C_L for particles depends on the rotational motion of the particle around its center. Some authors, because of this uncertainty, simply omit the lift term (Uchiyama, 1999)[13]. The effect that solid walls exert on its surrounding bubbles is included by means of a so-called wall force. Antal et al. (1991)[1] modeled this force considering spherical rigid bubbles, but a recent model (Larreteguy et al., 2002)[8] assumes deforming and elastic bubbles.

In this state of affairs it is interesting to go back to very simple flows and try to extract as much information as possible about the behavior of the model, starting with a model that satisfies physical constitutive principles (Drew & Lahey, 1979)[3]. Perhaps the simplest flow is laminar fully developed flow in a circular pipe. A decade ago Antal *et al* (1991)[1] reported on fully developed solutions of the two-fluid model equations. They solved the equations numerically for some specific data so as to reproduce experimental data from Nakoryakov *et al* (1986)[9]. Our objective here is to go beyond that analysis and explore generic properties of the two-fluid model equations (and solutions) under fully developed conditions.

The two-fluid model is briefly recalled in Section 2. Section 3 is devoted to algebraic manipulations of the equations. We arrive at a single ordinary differential equation (ODE), which is rendered non-dimensional by introducing an intrinsic length scale L, of the order of the bubble's radius. The solutions of this ODE are easily investigated using *Mathematica* (Wolfram, 1991)[15] since far from the wall no non-dimensional number is involved. It turns out that for pipes with diameter greater than about $20L$ no physically meaningful solution exists other than flat void fraction and velocity profiles. This comes from an exact compensation of the applied pressure gradient with the hydrostatic force $\rho_{\text{eff}}\,\mathbf{g}$, where ρ_{eff} is the effective density of the mixture and $\mathbf{g}$ the acceleration of gravity.

Finally, Section 4 contains the results of a numerical approach similar to that of Antal *et al* (1991)[1]. In our case, the presentation focuses on the confirmation of the results of Section 3 once wall effects are introduced by means of a wall force. The numerical approach also allows us to extend the study to the regimes where regions of strictly zero void fraction are predicted.

2 THE TWO-FLUID MODEL

We consider the mass and momentum conservation equations neglecting temperature effects (Drew & Passman, 1999)[5],

$$\frac{\partial(\epsilon_k \rho_k)}{\partial t} + \nabla \cdot (\epsilon_k \rho_k \vec{v}_k) = 0 \quad , \tag{1}$$

$$\frac{\partial(\epsilon_k \rho_k \vec{v}_k)}{\partial t} + \nabla \cdot (\epsilon_k \rho_k \vec{v}_k \vec{v}_k) = \nabla \cdot [\epsilon_k (T_k + \tau_k^{\mathrm{Re}})] + \epsilon_k \rho_k \vec{g} + M_k \quad , \tag{2}$$

in which k refers to the phase (L for liquid, G for gas), ϵ_k is the volumetric fraction of phase k, $\vec{v}_k$ the corresponding velocity, ρ_k the density, T_k the stress tensor,

$$T_k = -p_k I + \mu_k [\nabla \vec{v}_k + (\nabla \vec{v}_k)^T] \quad ,$$

p_k the pressure, and μ_k the viscosity. τ_k^{Re} is the Reynolds-like stress due to statistical fluctuations, modeled by (Nigmatulin, 1979)[10] :

$$\tau_L^{\mathrm{Re}} = -\epsilon_G \, \rho_L \left[A |\vec{v}_G - \vec{v}_L|^2 I + B (\vec{v}_G - \vec{v}_L)(\vec{v}_G - \vec{v}_L) \right] \quad , \tag{3}$$

where customary values for A and B are $\frac{3}{20}$ and $\frac{1}{20}$, respectively. We denote hereafter $\vec{v}_G - \vec{v}_L$ by $\vec{v}_r$, and define $v_r = |\vec{v}_r|$.

In (2), M_k stands for the interfacial momentum exchange, which relates to the actual force between phases (M'_k) according to

$$M_k = p_{ki} \nabla \epsilon_k - \tau_{ki} \cdot \nabla \epsilon_k + M'_k \quad , \tag{4}$$

where subscript i refers to values at the interphase. Different models exist for M_k, in particular for the liquid phase ($k = L$),

$$M_L = p_{Li} \nabla \epsilon_L - \left[\mu_L \left(\nabla v_L + \nabla v_L^T \right) - \rho_L \left(A |\vec{v}_r|^2 I + B (\vec{v}_r \cdot \vec{v}_r) \right) \right] \nabla \epsilon_L + M'_L \quad \text{(Antal, 1991)}^1, \tag{5}$$

$$M_L = p_{Li} \nabla \epsilon_L - \left[\rho_L \left(ab \, |\vec{v}_r|^2 I - a^2 (\vec{v}_r \cdot \vec{v}_r) \right) \right] \nabla \epsilon_L - \rho_L \epsilon_L \nabla \cdot (\vec{v}_r \cdot \vec{v}_r) + M'_L \quad \text{(Drew \& Passman, 1999)}^5, \tag{6}$$

where $a = -\frac{9}{20}$ and $b = \frac{3}{20}$.

The pressure at the interphase (p_{Li}) can be derived from the expression (Stuhmiller, 1977)[12] :

$$p_L - p_{Li} = C \, \rho_L \, \epsilon_L \, |\vec{v}_r|^2 \quad , \quad C = \frac{1}{4} \quad . \tag{7}$$

We will consider drag, lift and wall forces, $M'_k = M'^D_k + M'^L_k + M'^W_k$, with

$$M'^D_G = -M'^D_L = -\frac{3}{8} \frac{\epsilon_G}{R_b} C_D \, \rho_L \vec{v}_r |\vec{v}_r| \quad , \tag{8}$$

$$C_D = \frac{24}{Re}(1 + 0.1\ Re^{0.75}) \quad , \quad Re = \frac{2R_b\ \rho_L|\vec{v}_r|}{\mu_m} \quad , \quad \mu_m = \frac{\mu_L}{(1-\epsilon_G)} \quad , \tag{9}$$

$$M_G'^L = -M_L'^L = -C_L\ \epsilon_G\ \rho_L \vec{v}_r \wedge (\nabla \wedge \vec{v}_L) \quad , \tag{10}$$

$$M_G'^W = -M_L'^W = \frac{\epsilon_G\ \rho_L |u_\parallel|^2}{R_b}\left[C_{W1} + C_{W2}\left(\frac{R_b}{y_0}\right)\right]\breve{n}_w \quad , \tag{11}$$

$$u_\parallel = \vec{v}_r - [\breve{n}_w \cdot \vec{v}_r]\breve{n}_w \quad , \quad C_{W1} = -0.1 \quad , \quad C_{W2} = 0.147 \quad , \tag{12}$$

where y_0 is the distance to the wall, $\breve{n}_w$ the exterior unit normal and R_b the bubble radius.

Considering fully developed flow in a vertical cylindrical duct, the complete set of equations presented can be summarized in a system of five differential equations corresponding to five unknown functions, i.e. $v_L(r)$, $v_G(r)$, $p_L(r,z)$, $p_G(r,z)$ and $\epsilon_G(r)$, as follows :

• Momentum conservation equation - gas phase - radial direction ($\breve{r}$)

$$\epsilon_G\left[\frac{\partial p_G}{\partial r} + C_L\ \rho_L\ v_r \frac{\partial v_L}{\partial r} + \frac{\rho_L\ v_r^2}{R_b}(C_{W1} + C_{W2}\frac{R_b}{(R-r)})\right] = 0 \quad , \tag{13}$$

where R is the internal radius of the duct.

• Momentum conservation equation - gas phase - axial direction ($\breve{z}$)

$$\frac{\partial p_G}{\partial z} = -\rho_G\ g - \frac{3}{8}\frac{C_D}{R_b}\rho_L\ v_r|v_r| \quad . \tag{14}$$

This equation is used for the calculation of the relative velocity (v_r). This velocity will hereafter be considered uniform. This is a good aproximation, considering the fact that the only and weak dependence of this equation on the radial coordinate remains on the drag coeficient (C_D).

• Momentum conservation equation - liquid phase - radial direction ($\breve{r}$)

$$\begin{aligned}\epsilon_L\frac{\partial p_L}{\partial r} = &-\frac{\partial}{\partial r}\left[A\ \rho_L\ \epsilon_L(1-\epsilon_L)v_r^2\right] + C_L\ \epsilon_G\ \rho_L\ v_r\frac{\partial v_L}{\partial r} + C\ \rho_L(1-\epsilon_G)v_r^2\frac{\partial \epsilon_G}{\partial r} \\ &+\frac{\epsilon_G\ \rho_L\ v_r^2}{R_b}\left[C_{W1} + C_{W2}\frac{R_b}{(R-r)}\right] - C_1\ \rho_L\ v_r^2\frac{\partial \epsilon_G}{\partial r} \quad .\end{aligned} \tag{15}$$

• Momentum conservation equation - liquid phase - axial direction ($\breve{z}$)

$$\epsilon_L\frac{\partial p_L}{\partial z} = \frac{1}{r}\frac{\partial}{\partial r}\left[r\ \epsilon_L\ \mu_L\frac{\partial v_L}{\partial r}\right] + \frac{3}{8}\frac{\epsilon_G}{R_b}C_D\ \rho_L\ v_r|v_r| - \epsilon_L\ \rho_L\ g + C_2\ \mu_L\frac{\partial v_L}{\partial r}\frac{\partial \epsilon_G}{\partial r} \quad . \tag{16}$$

• Jump condition at the interphase

$$p_G - p_L = \frac{2\sigma}{R_b} - C\ \rho_L(1-\epsilon_G)v_r^2 \quad . \tag{17}$$

3 SYSTEM REDUCTION, SCALING AND GENERIC PROPERTIES OF THE SOLUTIONS

Let us define

$$\rho \equiv \rho_{\text{eff}} = \epsilon_L\, \rho_L + \epsilon_G\, \rho_G \quad , \quad \overline{\rho} \equiv \frac{1}{S}\int_S \rho\, dS \quad , \quad \frac{\partial P}{\partial z} \equiv \frac{\partial p}{\partial z} + \overline{\rho} g \quad , \tag{18}$$

where S is the cross-sectional area of the pipe.

Eliminating the drag force from (14) and (16), and using $\epsilon_L = (\rho - \rho_G)/(\rho_L - \rho_G)$, one arrives at

$$\frac{\partial P}{\partial z} + (\rho - \overline{\rho})g = \frac{(\rho - \rho_G)}{(\rho_L - \rho_G)}\frac{\mu_L}{r}\frac{\partial}{\partial r}\left(r\frac{\partial v_L}{\partial r}\right) + (C_2 - 1)\mu_L \frac{\partial v_L}{\partial r}\frac{\partial \epsilon_G}{\partial r} \quad . \tag{19}$$

Replacing (15) and (17) into (13) one obtains, after multiplication by $\epsilon_L/(\rho_L\, v_r)$,

$$\begin{aligned}\frac{(\rho - \rho_G)}{(\rho_L - \rho_G)}\frac{1}{(\rho_L - \rho_G)}\frac{\partial \rho}{\partial r} &= \frac{C_L}{(2C - A)v_r}\frac{\partial v_L}{\partial r} + \frac{1}{R_b\,(2C - A)}(C_{W1} + C_{W2}\frac{R_b}{R - r}) \\ &\quad - \frac{(C_1 + A\,\epsilon_G)}{(2C - A)}\frac{1}{(\rho_L - \rho_G)}\frac{\partial \rho}{\partial r} \quad .\end{aligned} \tag{20}$$

The system is thus reduced to only two equations, which motivates the introduction of the following non-dimensional (scaled) variables:

$$\frac{\partial P^*}{\partial z} \equiv \frac{1}{(\rho_L - \rho_G)g}\frac{\partial P}{\partial z} \quad , \quad L^2 \equiv \frac{2\,\mu_L\, v_r (C - A)}{g(\rho_L - \rho_G)C_L} \quad , \quad v^* = \frac{v_L}{v_r}\frac{C_L}{2(C - A)} \quad , \tag{21}$$

$$r^* \equiv \frac{r}{L} \quad , \quad R^* \equiv \frac{R}{L} \quad , \quad R_b^* \equiv \frac{R_b}{L} \quad , \quad E \equiv \frac{C_{W1}}{2(C - A)R_b^*} \quad , \quad D \equiv \frac{C_{W2}}{2(C - A)} \quad . \tag{22}$$

Table 1 shows values of the intrinsic length scale L calculated for different dispersed phases in stagnant water, assuming a constant bubble (or particle) radius of 0.5 mm and a lift coefficient $C_L = 0.1$. To leading order, L depends only on the bubble radius and on the model constants $C - A$ and C_L, and for reasonable values of these coefficients is of the order of the bubble radius.

From (19)-(20), using the scaled variables in (21)-(22) and considering the wall-force terms as null, the following ordinary differential equation is obtained :

$$\begin{aligned}&(\epsilon_L)^2\frac{\partial^2 \epsilon_L}{\partial r^{*2}} + (2 - C_2)\epsilon_L\left(\frac{\partial \epsilon_L}{\partial r^*}\right)^2 + \frac{(\epsilon_L)^2}{r^*}\frac{\partial \epsilon_L}{\partial r^*} - \epsilon_L + \\ &+\frac{(C_1 + A)}{2(C - A)}\left[\epsilon_L\left(\frac{1}{r^*}\frac{\partial \epsilon_L}{\partial r^*} + \frac{\partial^2 \epsilon_L}{\partial r^{*2}}\right) - (C_2 - 1)\left(\frac{\partial \epsilon_L}{\partial r^*}\right)^2\right] = \frac{\partial P^*}{\partial z} - \overline{\epsilon_L} \quad ,\end{aligned} \tag{23}$$

where $\overline{\epsilon_L} = (\overline{\rho} - \rho_G)/(\rho_L - \rho_G)$. The equation holds wherever the wall force is not active ($R - r > -\frac{D}{E}L$). Notice that the right-hand side is a constant, independent of r^*.

Mixture	$\rho_c\ (kg/m^3)$	$\mu_c\ (kg/(m\,s))$	$\rho_d\ (kg/m^3)$	$v_r\ (m/s)$	L (m)
water-air	998	0.001	1.19	0.1184	$1.557\ 10^{-4}$
water-CO_2	998	0.001	1.9022	0.1183	$1.557\ 10^{-4}$
water-polystirene	998	0.001	55	0.1143	$1.573\ 10^{-4}$
water-wood	998	0.001	545	0.0714	$1.793\ 10^{-4}$
water-oil	998	0.001	874	0.0297	$2.211\ 10^{-4}$
water-glass	998	0.001	2500	- 0.153	$1.442\ 10^{-4}$
water-steel	998	0.001	7900	- 0.387	$1.07\ 10^{-4}$
water-vapor	958.12	0.000282	0.598	0.1545	$0.964\ 10^{-4}$

Table 1: Some typical values of the length scale L. Subscript c refers to the continuous phase and subscript d to the dispersed phase. The water-vapor system is considered at 100 °C and atmospheric pressure. The bubble (or particle) radius was assumed as 0.5 mm .

We have fixed the values of the constants A and B at their usual values $A = \frac{3}{20}$, $B = \frac{1}{20}$, and considered two sets of values for C_1 and C_2, namely $C_1 = -\frac{3}{20}$ and $C_2 = 1$ taken from Antal *et al* (1991)[1] (Model I), or $C_1 = -\frac{27}{400}$ and $C_2 = 0$, taken from Drew & Passman (1999)[5] (Model II).

Adopting, for example, the model of Antal *et al*, Equation (23) is reduced to :

$$(\epsilon_L)^2 \frac{\partial^2 \epsilon_L}{\partial r^{*2}} + \epsilon_L \left(\frac{\partial \epsilon_L}{\partial r^*} \right)^2 + \frac{(\epsilon_L)^2}{r^*} \frac{\partial \epsilon_L}{\partial r^*} - \epsilon_L = \frac{\partial P^*}{\partial z} - \overline{\epsilon_L} \quad , \tag{24}$$

which in some sense is the "universal" equation of laminar fully developed bubbly flow far from the wall, in the sense that it contains no parameters except for the constant on the right-hand side. Different solutions of (24) are obtained by changing two parameters: the pressure gradient and the amount of gas in the flow. For the analysis that follows we will change the second parameter for the liquid fraction at $r^* = 0$, $\epsilon_L(0)$, and will rewrite the right-hand side of (24) as

$$\frac{\partial P^*}{\partial z} - \overline{\epsilon_L} = -\epsilon_L(0)(1+\lambda) \quad , \tag{25}$$

finally resulting in

$$(\epsilon_L)^2 \frac{\partial^2 \epsilon_L}{\partial r^{*2}} + \epsilon_L \left(\frac{\partial \epsilon_L}{\partial r^*} \right)^2 + \frac{(\epsilon_L)^2}{r^*} \frac{\partial \epsilon_L}{\partial r^*} - \epsilon_L = -\epsilon_L(0)(1+\lambda) \quad . \tag{26}$$

If the model of Drew & Passman is adopted, an analogous equation is derived :

$$\begin{aligned} (\epsilon_L)^2 \frac{\partial^2 \epsilon_L}{\partial r^{*2}} + 2\epsilon_L \left(\frac{\partial \epsilon_L}{\partial r^*} \right)^2 + \frac{(\epsilon_L)^2}{r^*} \frac{\partial \epsilon_L}{\partial r^*} - \epsilon_L + \\ + \frac{33}{80} \left[\epsilon_L \left(\frac{1}{r^*} \frac{\partial \epsilon_L}{\partial r^*} + \frac{\partial^2 \epsilon_L}{\partial r^{*2}} \right) + \left(\frac{\partial \epsilon_L}{\partial r^*} \right)^2 \right] = -\epsilon_L(0)(1+\lambda) \quad . \end{aligned} \tag{27}$$

We thus solve ODE (26)-(27) with initial conditions $\epsilon_L(0)$ given and $\epsilon'_L(0) = 0$, for different constant right-hand sides which we parameterize with λ. Notice that

$$\frac{\partial p_L}{\partial z} = -\rho(0)g - \lambda[(1 - \epsilon_G(0))(\rho_L - \rho_G)g] \quad , \tag{28}$$

so that λ is a measure of the difference between the applied pressure gradient and the effective weight of the mixture at the center of the pipe.

Equations (26)-(27) are then solved using *Mathematica* (Wolfram, 1991)[15] for a wide set of values of the parameters $\epsilon_L(0)$ (equal to $1 - \epsilon_G(0)$) and λ. Some solutions can be found in Figs. 1 - 3.

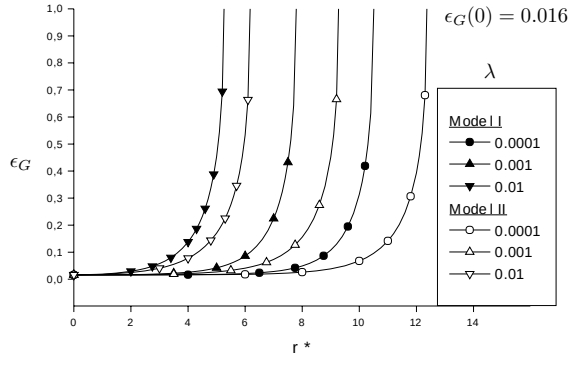

Figure 1: $\epsilon_G(r^*)$ - $\lambda > 0$ - Upward flow

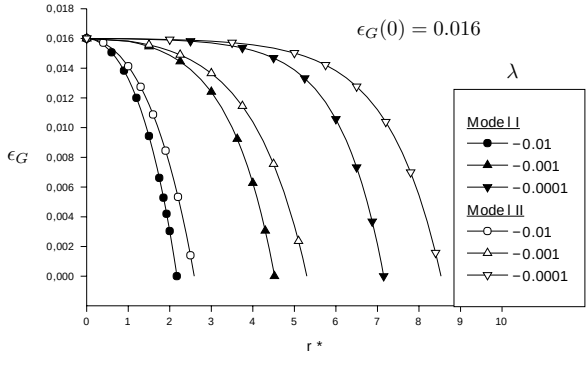

Figure 2: $\epsilon_G(r^*)$ - $\lambda < 0$ - Downward flow

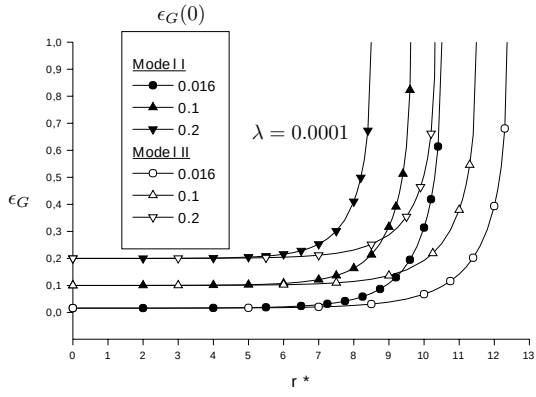

Figure 3: $\epsilon_G(r^*)$ for different $\epsilon_G(0)$

A generic fact about the biparametric family of solutions of (26)-(27) is that there exists a limit value of r^*, which we will denote *critical radius* r_c^*, at which ϵ_L becomes unphysical (either negative or greater than one). In Fig. 4 we plot r_c^* as a function of $|\lambda|$ for different values of $\epsilon_G(0)$. Consider for example the plot with $\epsilon_G(0) = 0.016$. Remember that the length scale is of the order of R_b, and to fix ideas assume that the radius of the pipe you are dealing with is 40 times R_b. This is indeed a small-diameter pipe. However, from Fig. 5 it is evident that *unless* $|\lambda| < 10^{-6}$ *there exists no solution to the governing equations* (26)-(27) *that remains between 0 and 1 throughout the section of the pipe*. In all reasonable cases (that is, pipes that are significantly bigger than the bubble radius) the band of "allowed" values for λ, which is centered at zero, is extremely narrow. What does this mean? It means that in fully developed laminar flow the solutions of the two-fluid model (the *only physically meaningful solutions that exist*) are such that the effective weight at the center of the pipe (i.e., $\rho_{\text{eff}}\,\vec{g}$) practically balances the applied pressure gradient. By "practically" we mean that the difference, as in the example above, is one part per million or less.

This striking result allows us to prove, as a corollary, that:

Consequence 1: The flat *void fraction* profiles typical of two-phase pipe flow are the only possible solutions of the two-fluid model (unless the diameter of the pipe is too small).

This can be proved simply by inspecting the solutions of (26)-(27) which have $|\lambda| < 10^{-6}$, and confirming that all of them are extremely flat (as functions of r^*) until very close to r_c^*, at which point they exhibit a rapid growth (if λ is positive) or decrease (if λ is negative) that take the value of ϵ_G above one or below zero. Another, more heuristic way, of proving that void fraction profiles are necessarily flat, once we know that $|\lambda| < 10^{-6}$, comes from a term-by-term analysis of (26)-(27). The fact that $|\lambda|$ is small implies the "practical" cancelation, at $r^* = 0$, of the fourth term on the left-hand

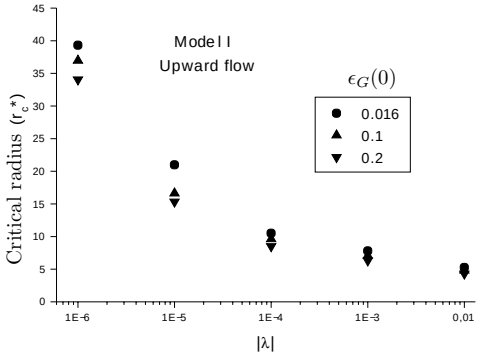

Figure 4: r_c^* as a function of $|\lambda|$ for different $\epsilon_G(0)$

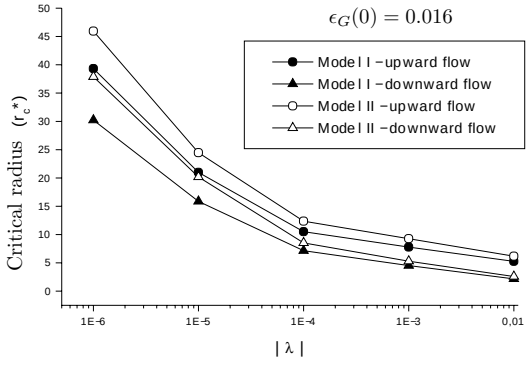

Figure 5: r_c^* as a function of $|\lambda|$

side of (26)-(27) with its right-hand side. This leaves us with the remaining terms, all of them containing derivatives of ϵ_L, equated to zero ("practically") and with the boundary condition $\epsilon_L'(0) = 0$. The solution to this problem is (again "practically", in the sense already explained) a constant, and thus a flat void fraction profile.

This is not the only consequence of λ being necessarily very small.

Consequence 2: The flat void fraction profile away from the wall of the pipe has a value of ϵ_L (and thus of ϵ_G) that only depends on the applied pressure gradient, the density of the phases, and the gravity. In particular, the value of ϵ_G does *not* depend on (a) the gas flow rate, (b) the viscosity of the phases, or (c) the slip velocity. The proof is immediate from (28).

Once $\epsilon_L(r^*)$ is obtained, the equation

$$-\epsilon_L(0)(1+\lambda) = \epsilon_L \frac{1}{r^*}\frac{\partial}{\partial r^*}\left(r^*\frac{\partial v^*}{\partial r^*}\right) - \epsilon_L \quad , \tag{29}$$

with initial condition $\frac{dv_L^*}{dr^*}(r^*=0)=0$, yields the liquid velocity up to a constant (the value at the center). It is again solved using *Mathematica*, with some sample results shown in Figs. 6 and 7.

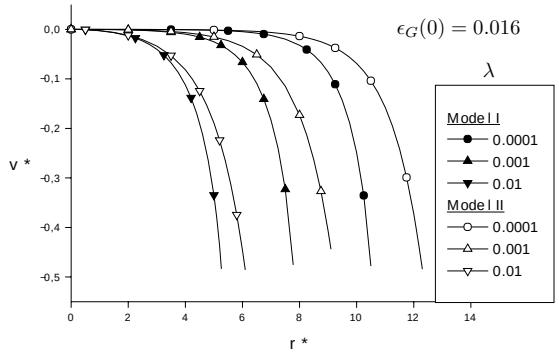

Figure 6: $v^*(r^*)$ - $\lambda > 0$ - upward flow

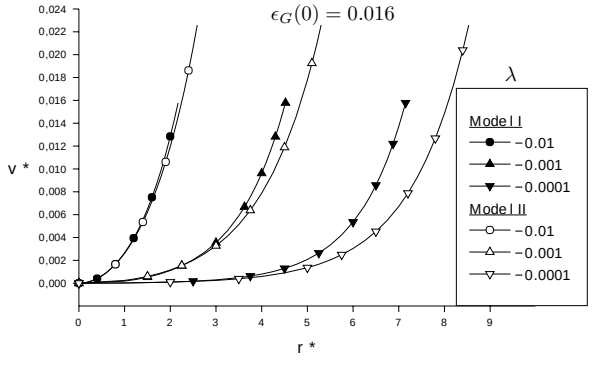

Figure 7: $v^*(r^*)$ - $\lambda < 0$ - downward flow

With a proof analogous to that of Consequence 1 we get :

Consequence 3: The flat *velocity* profiles typical of two-phase pipe flow are the only possible solutions of the two-fluid model (unless the diameter of the pipe is too small). In

particular, the flatness of two-phase laminar flow is *not* linked to turbulent-like effective stresses. It simply arises from an balance of the pressure gradient with the effective weight of the fluid column.

Remarkably, though our analysis concerns the equation without the wall-force terms, we can conclude about near-wall void-fraction profiles. The consequence is thus independent of the wall-bubble interaction model :

Consequence 4: In upward bubbly flows there must exist a so-called "peak" in the void fraction in the close vicinity of the wall.

The proof is not difficult. It is evident that, for the gas-liquid mixture to flow upward, the applied pressure gradient must overcome the horizontally-averaged weight $\overline{\rho}\,\vec{g}$, or, in non-dimensional variables, we must have : $-\frac{\partial P^*}{\partial z} > \overline{\epsilon_L}$.

But, since λ is very small, $-\frac{\partial P^*}{\partial z} \simeq \epsilon_L(0)$, leading to $\epsilon_L(0) > \overline{\epsilon_L}$ and thus to $\epsilon_G(0) < \overline{\epsilon_G}$. On the other hand, we know that ϵ_G is (practically) constant except very near the pipe wall. Thus, in most of the flow ϵ_G takes the value $\epsilon_G(0)$ which is *less* than the mean void fraction. It is obvious that a significant accumulation of bubbles must take place at the wall, leading to a "peak" in the void fraction.

In the case $C < A$, the affected terms in the scaled equation change sign, yielding (Model I) :

$$-(\epsilon_L)^2\frac{\partial^2\epsilon_L}{\partial r^{*2}} - \epsilon_L\left(\frac{\partial\epsilon_L}{\partial r^*}\right)^2 - \frac{(\epsilon_L)^2}{r^*}\frac{\partial\epsilon_L}{\partial r^*} - \epsilon_L = -\epsilon_L(0)(1+\lambda) \quad , \tag{30}$$

which accumulates bubbles at the center of the pipe in upward flow, just as if the lift were negative. It is remarkable that coefficients A (related to the effective Reynolds-like stress) and C (related to the interphase pressure correction) are mathematically linked in such a strong way. One cannot switch on and off the coefficients A and C arbitrarily, since their difference is as important as the lift coefficient itself.

4 NUMERICAL SIMULATION AND PARAMETRIC STUDY

The analysis of the previous section refers to the region where the wall forces are not active. Moreover, not all applied pressure gradients have been considered, since when $-\frac{\partial p_L}{\partial z}$ is greater than $\rho_L g$ the pressure gradient *cannot* be balanced by adjusting the void fraction at the center, even if the void fraction there is strictly zero. In the present section we report on some numerical studies made using finite elements to understand further the behavior of the system.

Eliminating the drag term from Eqs. (14) and (16), the differential equation for $v_L(r)$ results :

$$\frac{\partial p_L}{\partial z} + (1-\epsilon_G)\rho_L g + \epsilon_G\rho_G g = \frac{1}{r}\frac{\partial}{\partial r}\left[r\,(1-\epsilon_G)\,\mu_L\frac{\partial v_L}{\partial r}\right] + C_2\,\mu_L\frac{\partial v_L}{\partial r}\frac{\partial\epsilon_G}{\partial r} \quad . \tag{31}$$

Combining Eqs. (13), (15) and (17), and after mathematical manipulation, the differ-

ential equation for $\epsilon_G(r)$ results :

$$\epsilon_G \frac{\partial \epsilon_G}{\partial r}\, v_r^2 \left[(\frac{1}{2} - A + C_1) - \frac{1}{5}\epsilon_G \right] = -\epsilon_G C_L\, v_r \frac{\partial v_L}{\partial r} - \epsilon_G (C_{w1} + C_{w2}\frac{R_b}{R-r})\frac{v_r^2}{R_b} \quad . \tag{32}$$

The following boundary conditions are imposed to the system :

$$\frac{\partial v_L}{\partial r}(0) = 0 \quad , \quad v_L(R) = 0 \quad , \quad \frac{\partial \epsilon_G}{\partial r}(0) = 0 \quad , \tag{33}$$

with the aditional requirement :

$$\frac{1}{S}\int_S \epsilon_G \, dS \;=\; \overline{\epsilon_G} \quad , \quad \text{where } \overline{\epsilon_G} \text{ is given} \quad . \tag{34}$$

4.1 Numerical method

Equations (31) and (32) have been slightly modified in order to simplify their numerical treatment.

We add to both equations a time derivative term. Although we are considering a stationary case, treating it as transient allows the variables to adapt to their final value in a progressive and numerically more stable way.

We also add an artificial diffusion term to avoid undershoots that would lead to negative values of ϵ_G.

The resulting system is, thus :

$$\rho_L \frac{\partial v_L}{\partial t} + \frac{\partial p_L}{\partial z} + (1-\epsilon_G)\rho_L g + \epsilon_G \rho_G g = \frac{1}{r}\frac{\partial}{\partial r}\left[r\,(1-\epsilon_G)\,\mu_L \frac{\partial v_L}{\partial r} \right] + C_2\,\mu_L \frac{\partial v_L}{\partial r}\frac{\partial \epsilon_G}{\partial r}, \tag{35}$$

$$\begin{aligned} \frac{\partial \epsilon_G}{\partial t} + \epsilon_G \frac{\partial \epsilon_G}{\partial r} v_r^2 \left[(\frac{1}{2} - A + C_1) - \frac{1}{5}\epsilon_G \right] - K\frac{\partial^2 \epsilon_G}{\partial r^2} = \\ -\epsilon_G C_L v_r \frac{\partial v_L}{\partial r} - \epsilon_G (C_{w1} + C_{w2}\frac{R_b}{R-r})\frac{v_r^2}{R_b} \quad , \end{aligned} \tag{36}$$

where K is the artificial diffusion coefficient.

The time-marching scheme is semi-implicit :

$$\begin{aligned} \rho_L \frac{v_L^n - v_L^{n-1}}{\Delta t} + \frac{\partial p_L}{\partial z} + (1-\epsilon_G^{n-1})\rho_L g + \epsilon_G^{n-1}\rho_G g = \frac{1}{r}\frac{\partial}{\partial r}\left[r\,(1-\epsilon_G^{n-1})\,\mu_L \frac{\partial v_L^n}{\partial r} \right] \\ + C_2\,\mu_L \frac{\partial v_L^n}{\partial r}\frac{\partial \epsilon_G^{n-1}}{\partial r} \quad , \end{aligned} \tag{37}$$

$$\begin{aligned} \frac{\epsilon_G^{n*} - \epsilon_G^{n-1}}{\Delta t} + \epsilon_G^{n-1}\frac{\partial \epsilon_G^{n*}}{\partial r}\, v_r^2 \left[(\frac{1}{2} - A + C_1) - \frac{1}{5}\epsilon_G^{n-1} \right] + \epsilon_G^{n*} (C_{w1} + C_{w2}\frac{R_b}{R-r})\frac{v_r^2}{R_b} \\ - K\frac{\partial^2 \epsilon_G^{n*}}{\partial r^2} = -\epsilon_G^{n-1} C_L v_r \frac{\partial v_L^{n-1}}{\partial r} \quad , \end{aligned} \tag{38}$$

where ϵ_G^{n*} is an intermediate variable that, at every time step, is corrected to satisfy the condition (34) :

$$\epsilon_G^n = \epsilon_G^{n*} + (\overline{\epsilon_G} - \overline{\epsilon_G^{n*}}) \quad . \tag{39}$$

Defining :

$$G = \epsilon_G^{(n-1)}\, v_r^2 \left[(\frac{1}{2} - A + C_1) - \frac{1}{5}\epsilon_G^{(n-1)} \right] \quad , \quad H = (C_{w1} + C_{w2}\frac{R_b}{R-r})\frac{v_r^2}{R_b} \quad , \tag{40}$$

in Equation (38), G plays the role of a "velocity" and H the role of a "reaction". The diffusion coefficient K is thus selected as usual for reaction-convection problems (e.g. Codina, 1998)[2]:

$$K = \begin{cases} G\,h & ; \quad \text{if } H\,h^2 \le G\,h \\ H\,h^2 & ; \quad \text{if } H\,h^2 > G\,h \end{cases} \quad . \tag{41}$$

In this article, from now on, we will use the Drew & Passman model (Model II). Although the Antal *et al* model renders very similar results, it does not conserve the momentum in the axial direction.

4.2 Comparison with experimental data

In order to verify the numerical model, its results are compared to the experimental data reported by Nakoryakov *et al* (1986)[9], as previously done by Antal *et al* (1991)[1].

Important parameters of the experiment are: - Flow : bubbly, laminar, vertical, upward - Mixture : air - water - Pressure : atmospheric - Pipe diameter : 1.5 cm - Bubble diameter: 0.87 mm - Reynolds number (liquid phase) : 1267 - Area average void fraction ($\overline{\epsilon_G}$) : 0.019.

The physical parameters are the following : $\rho_L = 1000\ \frac{kg}{m^3}$; $\rho_G = 1.19\ \frac{kg}{m^3}$; $\mu_L = 0.001\ \frac{kg}{m\,s}$; $\frac{\partial p}{\partial z}$ = - 9649 P/m .

For the simulation we used $C_L = 0.1$, $v_r = 0.1028\ \frac{m}{s}$, $\overline{\epsilon_G} = 0.019$.

Figure 8 shows the comparison of the void fraction profiles. As it was already pointed out, the profile in the central region of the pipe is flat (*Consequence 1*). The profile presents a peak close to the wall (*Consequence 4*) before going to zero under the effect of the wall force. The numerical void fraction at the center of the pipe is $\epsilon_G(0) = 0.0154332$, so that

$$-\frac{\partial p}{\partial z} = 9649\,\frac{P}{m} \;\approx\; [(1-\epsilon_G(0))\rho_L \,+\, \epsilon_G(0)\rho_G]\,g \;=\; 9648.935\,\frac{P}{m} \quad , \tag{42}$$

and *Consequence 2* is confirmed.

From (28) one gets $\lambda = 6.77 \times 10^{-6}$.

Figure 9 shows the predicted liquid velocity profile, which is indeed flat though no turbulence was considered.

Finally, the average liquid velocity was calculated, $\overline{v_L} = \frac{1}{A}\int_A v_L\, dA \;\approx 0.08215\ \frac{m}{s}$, and the resulting liquid phase Reynolds number was $Re = 1232.2$, close to the experimental value ($Re = 1267$).

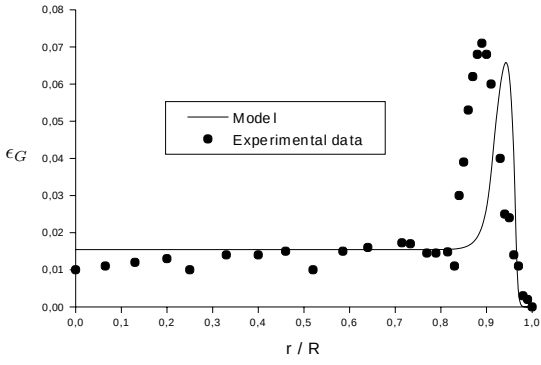

Figure 8: Void fraction profile

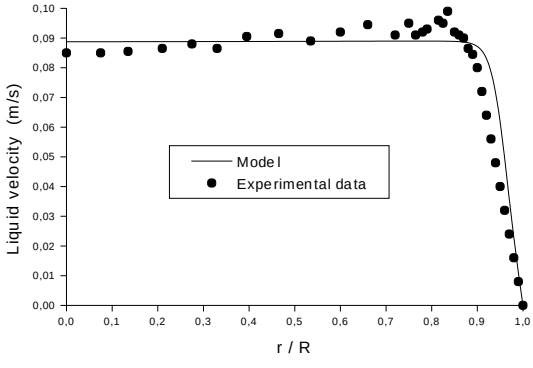

Figure 9: Liquid velocity profile

4.3 Parametric study

A parametric study was carried out using a general case, in order to analyze the behaviour of the main variables as a function of the applied pressure gradient and of the average void fraction ($\overline{\epsilon_G}$).

The parameters used are the following : $\rho_L = 1000\ \frac{kg}{m^3}$; $\rho_G = 1.19\ \frac{kg}{m^3}$; $\mu_L = 0.01\ \frac{kg}{m\ s}$; $C_L = 0.1$.

Figure 10 shows the void fraction profiles as a function of the applied pressure gradient, for upward flow and constant average void fraction $\overline{\epsilon_G}$. As the absolute value of the applied pressure gradient increases, the void fraction at the central region of the pipe diminishes, the peak increases its height and the radial position of the maximum moves towards the wall. This behaviour is due to an increasing lift force that obeys to an increasing liquid velocity gradient at the region close to the wall (see Figure 11).

From the results shown in Figure 10, another important conclusion can be drawn : *when* $-\frac{\partial p}{\partial z}$ *is equal or greater than the specific weight of the liquid phase* ($\rho_L\ g$)*, the void fraction at the central region becomes null.* Figures 12 and 13 show the void fraction and

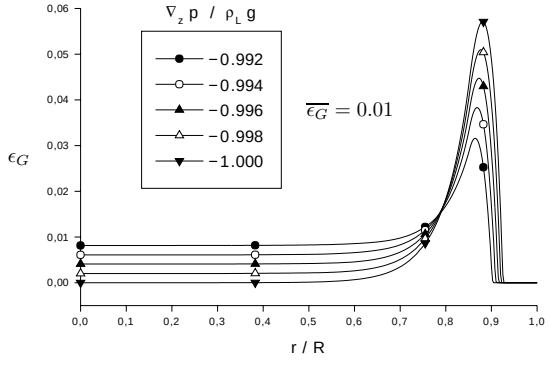

Figure 10: Void fraction profiles - Upward flow

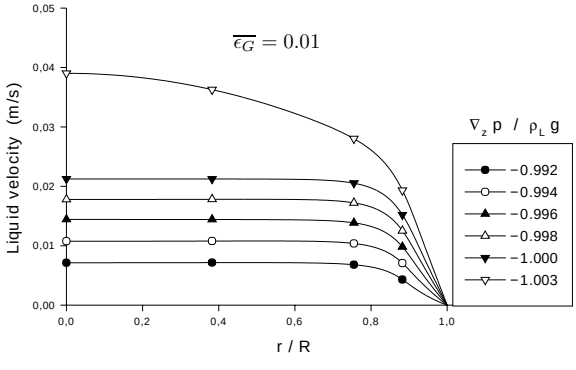

Figure 11: Liquid velocity profiles - Upward flow

velocity profiles for several applied pressure gradients, for downward flows. The lift force accumulates the bubbles at the central region, leaving a depleted zone close to the wall.

It has been previously demonstrated that λ is necessarily very small (Sec. 3). The parametric study allows us to verify and extend this conclusion : λ is very small ($|\lambda| \leq 10^{-6}$) when $\epsilon_G(0) \neq 0$ ($-\frac{\partial p}{\partial z} \leq \rho_L\ g$). When $\epsilon_G(0) = 0$ ($-\frac{\partial p}{\partial z} > \rho_L\ g$), λ depends linearly on the pressure gradient, as can be inferred from Equation (28). This is shown clearly in Figure 14 for different values of $\overline{\epsilon_G}$.

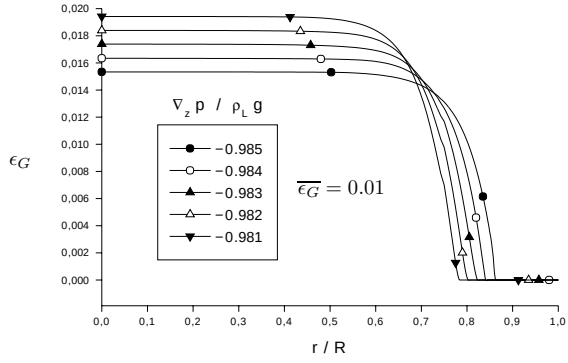

Figure 12: Void fraction profiles - Downward flow

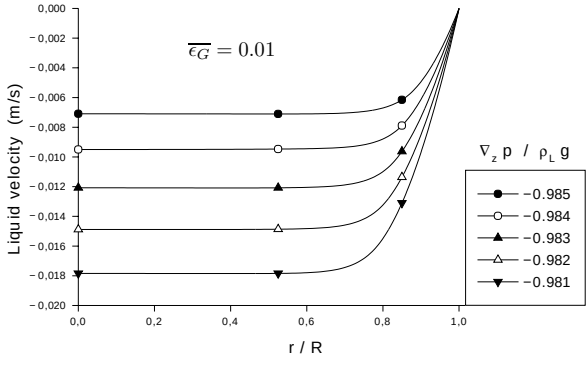

Figure 13: Liquid velocity profiles - Downward flow

Considering the fact that λ is very small, Equation (28) reduces to :

$$\frac{\partial p}{\partial z} = g\,(\rho_L - \rho_G)\,\epsilon_G(0) \;-\; g\,\rho_L \quad . \tag{43}$$

Notice that, in this case, $\epsilon_G(0)$ depends linearly on the applied pressure gradient (see Figure 15).

Figure 16 shows the total mass flow rate as a function of the applied pressure gradient, for different values of $\overline{\epsilon_G}$. As the absolute value of the applied pressure gradient increases, a proportional increase in the mass flow rate is observed. When the pressure gradient balances the specific weight of the liquid phase, a change of regime occurs: the flat velocity profile changes to a parabolic-type profile (see Figure 11), and the slope of the mass flow rate increases.

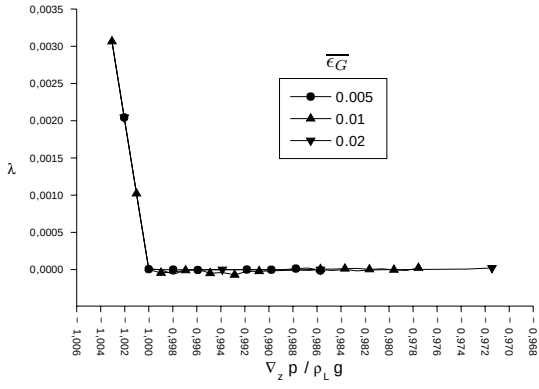

Figure 14: λ for different values of pressure gradient

5 CONCLUSIONS

An analysis of the two-fluid model solutions for the simple case of laminar fully-developed bubbly flow in a circular pipe has allowed us to identify several physical and mathematical properties of the flow.

All experimental results in bubbly flows show flat velocity and void-fraction profiles (Serizawa *et al* [11], 1986 ; Nakoryakov *et al* [9], 1986 ; Wang *et al* [14], 1987). The mathematical results of Section 3 have proved that, in laminar conditions, the flat profiles are the only valid solutions of the two-fluid model.

The numerical results of Sections 3 and 4 allowed us to obtain further insights into the physics of the flow. It was observed that the applied pressure gradient is balanced with the effective specific weight ($\rho_{\text{eff}}\,\mathbf{g}$) at the central region of the pipe , implying that the void fraction ($\epsilon_G(0)$) only depends on the applied pressure gradient. For high enough pressure gradients in upward flows this is no longer possible and a new flow regime appears with a pure-liquid core. In downward flows, on the other hand, the pure-liquid region occurs close to the walls and grows thicker with increasing flow rate.

Future work will be aimed at extending these results to the turbulent case, coupling the two-fluid model with a low-Reynolds-number $k-\varepsilon$ turbulent model.

ACKNOWLEDGMENTS : GCB is also a fellow of CONICET, Argentina. Partial support was received from ANPCYT, Argentina, through grant PICT'99 No. 6337. Fruitful discussions with R. T. Lahey Jr., A. Larreteguy, F. Moraga and F. Bonetto are gratefully acknowledged. This paper is dedicated to the late Prof. Ben C. Yen. He was an inspiration to all of us who had the good fortune to be associated with him.

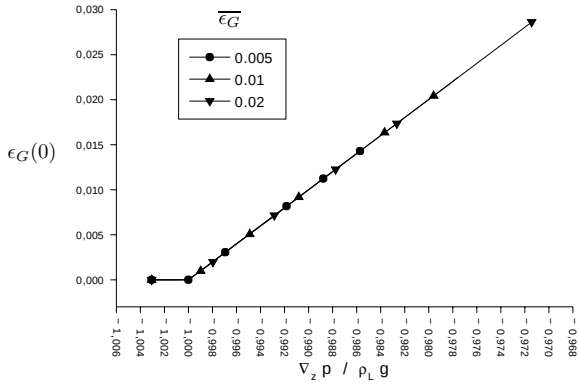

Figure 15: $\epsilon_G(0)$ for different values of pressure gradient

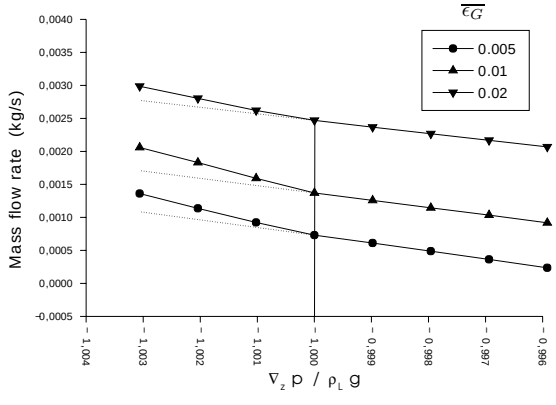

Figure 16: Mass flow rate for different values of pressure gradient

REFERENCES

[1] S. Antal, R. Lahey Jr, and J. Flaherty. Analysis of phase distribution in fully developed laminar bubbly two-phase flow. *Int. J. Multiphase Flow*, 17(5):635–652, 1991.

[2] R. Codina. A comparison of some finite element methods for solving the diffusion-convection-reaction equation. *Computer Methods in Applied Mechanics and Engineering*, 156:185–210, 1998.

[3] D. Drew and R. Lahey Jr. Application of general constitutive principles to the derivation of multidimensional two-phase flow equations. *Int. J. Multiphase Flow*, 5:243–264, 1979.

[4] D. Drew and R. Lahey Jr. The virtual mass and lift force on a sphere in rotating

and straining inviscid flow. *Int. J. Multiphase Flow*, 13(1):113–121, 1987.

[5] D. Drew and S. Passman. *Theory of Multicomponent Fluids*, volume 135 of *Applied Mathematical Sciences*. Springer, 1998.

[6] M. Ishii. *Thermo-fluid Dynamic Theory of Two-phase Flow*. Eyrolles, 1975.

[7] R. Lahey Jr. The analysis of phase separation and phase distribution phenomena using two-fluid models. *Nuclear Eng. and Design*, 122:17–40, 1990.

[8] A. Larreteguy, D. Drew, and R. Lahey Jr. A particle-centre-averaged two-fluid model for wall-bounded bubbly flows. In *Fifth International Symposium on Numerical Methods for Multiphase Flow at the 2002 ASME Fluids Engineering Division Summer Meeting*. The American Society of Mechanical Engineers, 2002.

[9] V. Nakoryakov *et al*. Study of upward bubbly flow at low liquid velocities. *Izv. sib. Otdel. Akad. Nauk SSSR.*, 16:15–20, 1986.

[10] R. Nigmatulin. Spatial averaging in the mechanics of heterogeneous and dispersed systems. *Int. J. Multiphase Flow*, 4:353–385, 1979.

[11] A. Serizawa, I. Kataoka, and I. Michiyoshi. Phase distribution in bubbly flow. *Proceedings of the Second International Workshop on Two-Phase Flow Fundamentals*, Data Set No. 24, 1986.

[12] J. Stuhmiller. The influence of interfacial pressure on the character of two-phase flow model equations. *ASME Symp. on computational techniques for non-equilibrium two-phase phenomena*, page 118, 1977.

[13] T. Uchiyama. Petrov-Galerkin finite element method for gas-liquid two-phase flow based on an incompressible two-fluid model. *Nuclear Eng. and Design*, 193:145–157, 1999.

[14] S. Wang, S. Lee, O. Jones Jr, and R. Lahey Jr. 3-D turbulence structure and phase distribution measurements in bubbly two-phase flows. *Int. J. Multiphase Flow*, 13(3):327–343, 1987.

[15] S. Wolfram. *Mathematica*. Addison-Wesley, 1991.